RAPID COMMUNICATIONS

PHYSICAL REVIEW B VOLUME 42, NUMBER 15 15 NOVEMBER 1990-II

Cyclotron effective mass in wide parabolic quantum wells

K. Karraï, M. Stopa, X. Ying, H. D. Drew, and S. Das Sarma
Joint Program for Advanced Electronic Materials, Department of Physics and Astronomy, University of Maryland, College Park, Maryland 20742 and Laboratory for Physical Sciences, College Park, Maryland 20740

M. Shayegan
Department of Electrical Engineering, Princeton University, Princeton, New Jersey 08544
(Received 8 June 1990)

Cyclotron-resonance measurements are reported for wide (100–300 nm) modulation-doped $Al_xGa_{1-x}As$ graded parabolic quantum wells for electron areal densities $N_S = 10^9/cm^2$–$2.5 \times 10^{11}/cm^2$. A clear dependence of the cyclotron frequency on N_S is observed in the extreme quantum limit which is understood in terms of alloy effects. Self-consistent calculations that include the x dependence of the local effective mass and exchange-correlation effects in a local-density approximation are in quantitative agreement with the measurements for high densities. At low densities a pinning of the cyclotron frequency is observed that is not predicted by the model.

Remotely doped wide parabolic quantum wells have been shown to produce a quasi-three-dimensional electron system with low disorder.[1–13] These electron systems are of considerable interest since they are an example of a strongly interacting electron gas embedded in a jellium background, in which a variety of collective excitations are predicted to occur.[14] The spatial dependence of the electrostatic potential due to a homogeneous positive jellium background charge distribution is quadratic. An effective parabolic potential is produced by growing a spatially graded $Al_xGa_{1-x}As$ heterostructure by molecular-beam epitaxy. In order to tailor the conduction-band-edge to mimic a jellium potential, the Al concentration $x(z)$ is quadratically varied (i.e., a graded alloy) along the growth direction z. When the barrier regions surrounding the wells are n doped, a high-mobility electron gas of desired density is obtained in the parabolic confinement potential.[1–13] At high magnetic fields and low temperatures the optical response of this system to far-infrared radiation is very similar to that of a homogeneous three-dimensional (3D) electron plasma.[4–6] However, as a consequence of the spatial gradation of $Al_xGa_{1-x}As$, some novel deviations from the 3D-electron-plasma behavior are expected. The dependence of x along the growth axis leads not only to a parabolic confinement potential, but also to a spatial dependence of the effective mass $m^*(z)$, the Landé factor $g^*(z)$, the static dielectric constant $\epsilon_s(z)$, and the local-alloy-disorder scattering. In the range of interest ($0 < x < 0.4$), these parameters are monotonic functions of z and change substantially over the extent of the electron envelope function $\xi(z)$. As a result, the measurable quantities which can be obtained from far-infrared spectroscopy, such as the cyclotron mass, spin-splitting energies, and carrier lifetimes, will depend on the extent of the electron gas in the z direction and hence on the filling (i.e., electron areal density N_S) of the well. In this Rapid Communication, we present evidence of such deviations and their analyses.

Cyclotron resonance was measured in the extreme quantum limit (i.e., only one spin-split Landau level occupied) with a magnetic field **B** (0–9 T) applied parallel to the growth axis. In this (Faraday) geometry the electromagnetic wave, which is linearly polarized in the plane of the electron slab, propagates along the field axis. The cyclotron effective mass m_c^*, the electron areal density N_S, and the scattering time τ_c are obtained from the positions and line-shape analysis of the resonances using a classical Drude conductivity model.[15]

We have studied two samples in which the Al concentration x varies quadratically from $x = 0$ to $x \cong 0.15$ (sample *A*), $x \cong 0.08$ (sample *B*), at the edges of a 150-nm (sample *A*), 260-nm (sample *B*), wide $Al_xGa_{1-x}As$ layer sandwiched between two $Al_yGa_{1-y}As$ barriers of composition $y = 0.38$. The resulting potential corresponds to that of a homogeneous 3D positive background of charge density $n_0 = 2.3 \times 10^{16}/cm^3$ (sample *A*), $n_0 = 6.7 \times 10^{15}/cm^3$ (sample *B*). The Al-concentration profiles were measured by secondary-ion mass spectroscopy (SIMS).[16] The profile corresponding to the central region of the well of sample *A* is shown in the inset of Fig. 2 and is seen to be well approximated by a parabolic curve. For both samples we obtained n_0 by measuring the collective cyclotron resonance (plasma-shifted cyclotron resonance).[4–6] The widths of the wells were obtained from the SIMS measurements with an accuracy of ± 10 nm. Since the SIMS measurements are not sufficiently accurate to determine the absolute Al concentrations, the absolute quadratic dependence of $x(z)$ was deduced from the potential profile of the well, $V(z) = \frac{1}{2}(n_0 e^2/\epsilon_0 \epsilon) z^2$, the conduction-band offset Q_e[$\cong 0.60$ (Ref. 17) or $\cong 0.69 \pm 0.03$ (Ref. 18)] and the $Al_xGa_{1-x}As$ band-gap dependence $E_g(x) = 1512 + 1455x$ (meV).[19] For the static dielectric constant we take $\epsilon = 13$ independent of x (for our devices, the relative change of ϵ is only a few percent). For the local effective mass we take the effective-mass dependence on the Al mole fraction in $Al_xGa_{1-x}As$ [$m^*(x) = 0.067 + 0.0838x$] from Ref. 20 and the spatial $x(z)$ dependence obtained from $V(z) = Q_e[E_g(x) - E_g(0)]$. Magneto-

transport studies ($\mathbf{B}\|z$) carried out at low temperatures on both samples[10,11,13] have demonstrated quantization along z as manifested by the integer and fractional quantum Hall effects. In order to calculate the eigenstates for the well the Schrödinger equation must be solved self-consistently with the Poisson equation for the total potential. Because of the slow variation of $m^*(x)$ with respect to z, the effective-mass formalism remains appropriate for describing the electronic states of the system. Our calculations assume spinless electrons ($g^* \ll 1/m^*$) with the exchange-correlation potential calculated in the local density approximation, and includes the local effective-mass variation $m^*(z)$ in a BenDaniel and Duke type of Hamiltonian[21] in the presence of an external magnetic field. Details of our theory will be presented elsewhere.

A direct consequence of the spatial dependence $m^*(z)$ is the appearance of a discreet spectrum of cyclotron frequencies associated with electric- and magnetic-subband indices. This spectrum can be related to a set of effective masses (defined by $m^*_{cM,N} \equiv eB/\omega_{cM,N}$) which depend on the electron areal density and on the applied magnetic field. M and N are respectively the electric and magnetic subband indices. The cyclotron frequency $\omega_{cM,N}$ is defined by $\omega_{cM,N} = E_{M,N+1} - E_{M,N}$, where $E_{M,N}$ are eigenenergy levels of the system.

The cyclotron-resonance measurements were performed by laser spectroscopy. The far-infrared radiation was generated by an optically pumped molecular-gas laser. With laser wavelengths of 118.83 μm and 96.52 μm extreme quantum conditions were realized over the available N_S range. Qualitatively similar results were found for both frequencies. The radiation, which was propagated to the sample by light-pipe optics, was linearly polarized a few millimeters before the sample. The transmitted light was detected by a composite Ge bolometer located outside the magnetic field. The sample substrate was wedged 3° in order to avoid line-shape distortions due to interference fringes.[15] The sample was cooled from room temperatures down to 4.2 K over several hours in the dark. The electron areal densities were changed *in situ* by illumination with a red-light-emitting diode (LED) placed near the sample. Under illumination N_S reduces. After the LED is turned off, N_S rises slowly and eventually exceeds the original dark-cooled density. This effect has also been reported for GaAs heterojunctions.[22] The time scale for the saturation is hours at 1.5 K. Changing N_S by this technique has also been used for transport studies of these samples.[10]

The cyclotron-resonance spectra are shown for N_S between 3×10^{10} and $2.4\times10^{11}/\text{cm}^2$ in Fig. 1. The surface carrier concentration was deduced from an analysis of the cyclotron-resonance line shapes. Within the Drude approximation for a two-dimensional electron gas and assuming linearly polarized radiation, N_S is given by[15]

$$N_S = \epsilon_0 c(1+\sqrt{\epsilon})m^*/e^2 \frac{\Delta T \Delta B}{(1-2\Delta T)^{1/2}+1},$$

where ΔT is the maximum relative change in transmission and ΔB is the full linewidth at half maximum. The shape of the spectra is seen to change substantially as the electron density increases. We can distinguish between the

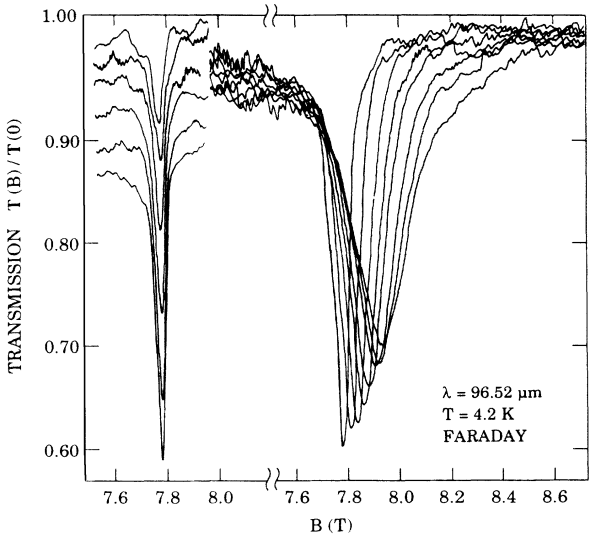

FIG. 1. Cyclotron-resonance spectra taken on sample A at $T=4.2$ K with the $\lambda=96.52$ μm laser line. The relative change of the transmitted-radiation intensity is shown as function of the magnetic field for different electron densities ranging from $N_S=3\times10^{10}$ to $2.4\times10^{11}/\text{cm}^2$. For clarity the low-density regime $N_S<8\times10^{10}/\text{cm}^2$ is shown separately on the left-hand side of the figure. In this regime the cyclotron frequency appears pinned.

behaviors in two different density regimes. As can be seen in Figs. 1 and 2, the cyclotron mass is nearly independent of N_S for $N_S \leq 8\times10^{10}/\text{cm}^2$ (sample A), $\leq 3\times10^{10}/\text{cm}^2$ (sample B). As N_S continues to increase, the cyclotron line shifts monotonically towards the higher effective cyclotron mass. The overall shift is a small effect when compared to the cyclotron frequency itself. The effect is substantial, however, when compared to the cyclotron linewidth because of the long cyclotron lifetime in these high-quality samples. The absolute accuracy of the cyclotron frequency ω_c has an uncertainty of $\simeq 1\%$ which is the accuracy of the magnetic-field calibration. Since the resonances were extremely sharp, however, the relative value of ω_c could be reproduced to better than 0.05%. This shift is represented in Fig. 2 in terms of the cyclotron effective-mass relative variation $\Delta m_c/m_c = [m_c(N_S) - m_{\min}]/m_{\min}$, where $m_{\min}$ is the minimum cyclotron mass in the measured density interval. We choose this relative representation because otherwise a theory-experiment comparison of the *absolute* high-field cyclotron masses would necessitate inclusion of band nonparabolicity.[23]

The theoretical results represented in Fig. 2 give the relative change of cyclotron effective mass associated with the lowest electric-subband level (i.e., $M=0$). In the higher-density regime the agreement with the experimental results is quite satisfactory. The increase of the cyclotron mass with electron density can be understood in simple terms. The electron envelope function $\xi(z)$ extends over regions of increasing z, and therefore x, as N_S increases. At low densities where $N_S < n_0 a_0$, the width of the charge density is well approximated by the zero motion $a_0 = (\hbar/m^*\omega_0)^{1/2}$ of the electrons in the empty parabolic well. For sample A the zero motion is $a_0 \cong 13$

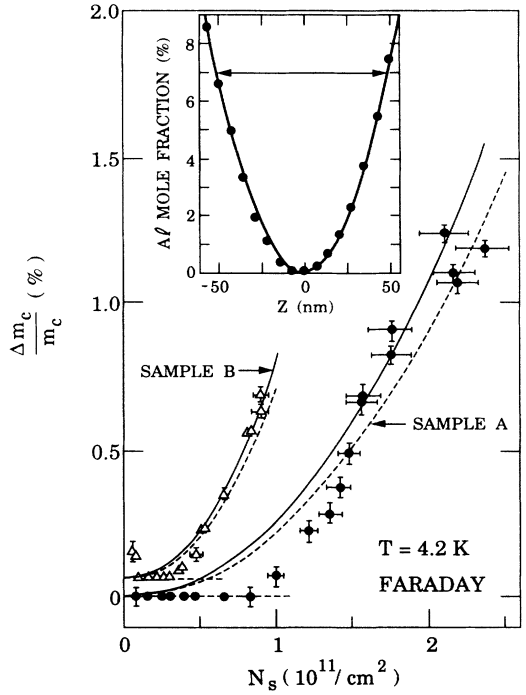

FIG. 2. The relative change of effective mass $[m_c(N_S) - m_{min}]/m_{min}$ for sample A (dots) using $\lambda = 96.52$ μm and sample B (triangles) using $\lambda = 118.83$ μm, measured as function of the areal electron density N_S. The solid and dashed lines are calculated, respectively, for $Q_e = 0.60$ and 0.69. The dotted horizontal lines, displaced vertically for clarity, indicate the pinning of the cyclotron resonance at low densities. Inset: The Al profile measured by SIMS on sample A in the central regin of the well (dots). The solid line is the closest parabolic fit. The horizontal arrow indicates the span of the electron-density distribution for the largest measured filling, $N_S = 2.4 \times 10^{11}/cm^2$.

nm. As seen from the inset of Fig. 2, x is well below 1% over the range of a_0 in the center of the well. In this regime, the cyclotron mass is expected to be nearly equal to the GaAs conduction-band mass. This is supported by our low-field low-density cyclotron-mass measurements in which case we found $m_c \cong 0.0670$ for sample B ($N_S = 5 \times 10^9/cm^2$). At high densities, the width of the charge-density distribution is well approximated by $L = N_S/n_0$.[4-6] For our maximum value of N_S in sample A, $L \cong 100$ nm, the extent of the distribution is represented by the horizontal arrow in the inset of Fig. 2. In that case the fraction of Al experienced by the electrons varies from 0% to 7% at the edges of the electron distribution. The cyclotron mass is then expected to correspond to that of an effective alloy of average Al composition $\bar{x} < 7\%$. In particular, for a classical electron gas in a parabolic well, this is $\bar{x} \cong x_{max}/3$.

In this classical limit is is straightforward to establish scaling relations for two samples of different curvatures and hence background densities n_A and n_B. $N_{SA}^2/N_{SB}^2 = n_A/n_B$ is the condition for which the cyclotron masses of both samples are equal. Equivalently $m_{cA}/m_{cB} = n_B/n_A$ is the condition obtained by setting the areal electron densities $N_{sA} = N_{sB}$. From these simple considerations we expect that for a given electron areal density the cyclotron mass is larger for the sample with the smaller background density (sample B). This is clearly illustrated in Fig. 2. This effect is quantitatively accounted for by our calculations as shown in Fig. 2 in the higher-density region. It is worth noting that all of the parameters introduced in the calculations are obtained from independent measurements, leaving no adjustable parameters.

In the lower-density region we note a clear theory-experiment discrepancy. As can be seen in Fig. 2, the measured cyclotron frequency is pinned, while the theory predicts a monotonic increase. The measured effect although only of the order of 0.1% is clearly observed. A more complete description should include the nonparabolicity (in the k-space sense) of the conduction band,[23] and the electron-longitudinal-optical-phonon interaction[24,25] (polaron). In parabolic wells both effects lead in principle to a reduction of the cyclotron mass as N_S increases. At the lowest densities the electrons have the largest kinetic energy (zero motion) contributing to a larger effective mass due to nonparabolicity. As N_S increases the kinetic energy decreases resulting in a reduction of the cyclotron mass. We estimated this nonparabolicity effect for both samples and found that it could not account for the observed pinning. The electron-phonon effect can lead to a reduction of mass with increasing N_S in two ways. First, as the width of the electron gas increases, the effective mass crosses over from a two-dimensional to a three-dimensional polaron-mass renormalization.[25] Second, the increase of the electron density leads to an increasing screening of the electron–LO-phonon interaction resulting in lowering the effective mass.[25] Both contributions act in a nontrivial way to compete with the alloy effect possibly leading to the observed pinning.

It is also noteworthy that an electron density of $2 \times 10^9/cm^2$ was obtained in sample B (under constant LED illumination) with a cyclotron lifetime of 15 ps. This is to our knowledge the lowest-density (high mobility) two-dimensional electron gas achieved at low temperatures in a semiconductor heterostructure. Under these conditions, however, the cyclotron frequency shifts to a lower frequency, as can be seen in Fig. 2. We do not understand this effect at this time. In addition to these effective-mass effects the cyclotron scattering times τ_c also were deduced from our data. We observed a dramatic dependence of the cyclotron lifetime on N_S. This can be seen qualitatively in Fig. 1 where the resonances broaden noticeably at higher N_S. The scattering time, deduced from the cyclotron resonance, was observed to peak for both samples, at $\tau_c = 5 \times 10^{-11}$ sec at $N_S = 8 \times 10^{10}/cm^2$ (sample A) and at $3 \times 10^{10}/cm^2$ (sample B). For higher densities τ_c decreases by a factor $\cong 3$. We related this reduction with the increasing alloy scattering that electrons experience as they spread out with increasing areal densities. A detailed analysis will be published elsewhere.

The discussion so far has been on the behavior of the lowest cyclotron resonance $\omega_{c0,0}$. We now turn to the cyclotron resonance $\omega_{c1,0}$ of the next higher electrical subband. Previous experimental results on similar quantum wells[4,9] have indicated the existence of two partly resolved cyclotron lines. In our earlier work[4] we failed to

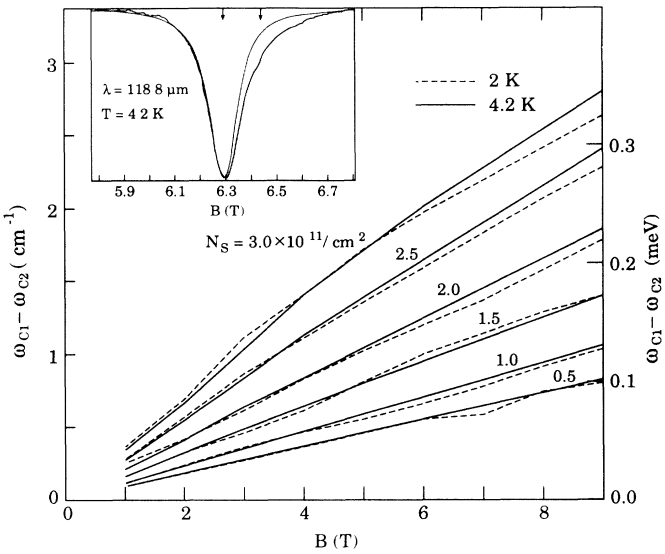

FIG. 3. The calculated splitting between the cyclotron frequencies of the two lowest electric subbands as function of B for various electron densities. Inset: The cyclotron resonance spectrum for $N_S = 2.4\times10^{11}/\text{cm}^2$ at $T = 4.2$ K. The two arrows indicate the calculated positions of the cyclotron resonances of two lowest electrical subbands. The spectrum is compared to a single Lorentzian line. The discrepancy found on the high-field side of the resonance may be accounted for by a weaker cyclotron resonance of the second electric subband.

explain the observed doublet in term of the spatial effective-mass variation in the well. The measured splitting was larger than expected by almost a factor of 2. In order to determine an experimental situation in which a second resonance may be observed we have calculated the energy splitting between the cyclotron resonances of the two lowest electric subbands. The results are shown in Fig. 3. They suggest that this splitting is larger at larger field and N_S. In the quantum limit only one subband is expected to be occupied at $T = 0$ K, however, the second electric subband can be thermally populated. At $N_S = 2.2\times10^{11}/\text{cm}^2$ the energy separation of the subband is only 1.1 meV so that a measurable thermal activation of the second subband is expected at 4.2 K. Unfortunately under the most favorable circumstances, $B = 8$ T and $N_S = 2.4\times10^{11}/\text{cm}^2$ (sample A), the calculated splitting is the same order as the measured cyclotron linewidth. The two resonances are, therefore, expected to be unresolved. Furthermore, under the assumption that the cyclotron lifetime is limited by alloy-disorder scattering, we have calculated that this second resonance is expected to be more than a factor of 3 wider than the fundamental cyclotron line. Indeed for temperature up to 20 K we did not find a second peak. However, as can be seen in the inset of Fig. 3, a noticeable asymmetry develops on the high-field side of the resonance at the highest values of the electron density. This is possibly due to the unresolved second electric-subband cyclotron resonance.

In conclusion, we have demonstrated the effect of the spatial dependence of the Al concentration in a wide parabolic $Al_xGa_{1-x}As$ quantum well on the cyclotron effective mass. While in the higher-density region we found a good agreement between the self-consistent calculations and the experimental results, the low-density region shows a puzzling discrepancy possibly related to electron-LO-phonon interaction. In addition, we have shown that an extended range of densities is accessible in these wide parabolic wells. This aspect allows the study of alloy-related effects over a variable range of x in the same sample.

We would like to thank M. Santos, T. Sajoto, and J. Jo for useful discussions and the sample growth. This work was supported by National Science Foundation Grants No. ECS-8553110, No. DMR-8705002, No. DMR-8704670 and U.S. Office of Naval Research Grants No. N00014-89-5-1551, No. N00014-89-J-1612, and No. N00014-88-K-0625.

[1]B. I. Halperin, Jpn. J. Appl. Phys. **26**, Suppl. 26-3, 1913 (1987).
[2]M. Sundaram *et al.*, Superlattices Microstruct. **4**, 683 (1988).
[3]M. Shayegan *et al.*, Appl. Phys. Lett. **53**, 791 (1988).
[4]K. Karraï *et al.*, Phys. Rev. B **39**, 1426 (1989).
[5]K. Karraï *et al.*, Phys. Rev. B **40**, 12020 (1989).
[6]K. Karraï *et al.*, Surf. Sci. **229**, 515 (1990).
[7]E. G. Gwinn *et al.*, Phys. Rev. B **39**, 6260 (1989).
[8]T. Sajoto *et al.*, J. Vac. Sci. Technol. B **7**, 311 (1989); T. Sajoto *et al.*, Phys. Rev. B **39**, 10464 (1989).
[9]A. Wixforth *et al.*, in *The Fourth International Conference on Modulated Semiconductor Structures, Ann Arbor, Michigan, 1989* [Superlattices Microstruct. (to be published)].
[10]T. Sajoto *et al.*, Appl. Phys. Lett. **55**, 1430 (1989).
[11]M. Shayegan *et al.*, Surf. Sci. **229**, 83 (1990).
[12]L. Brey, N. F. Johnson, and B. I. Halperin, Phys. Rev. B **40**, 10647 (1989).
[13]M. Shayegan *et al.* (unpublished).
[14]A. H. MacDonald and G. W. Bryant, Phys. Rev. Lett. **58**, 515 (1987).
[15]See, e.g., T. A. Kennedy *et al.*, Solid State Commun. **18**, 275 (1976).
[16]The SIMS measurements were done at Charles Evans and Associates, CA.
[17]R. C. Miller *et al.*, Phys. Rev. B **29**, 3740 (1984).
[18]J. Menendez and A. Pinczuk, IEEE J. Quantum. Electron. **24**, 1698 (1988).
[19]T. F. Kuech *et al.*, Appl. Phys. Lett. **51**, 505 (1987).
[20]M. Zachau *et al.*, Phys. Rev. B **33**, 8564 (1986).
[21]D. J. BenDaniel and C. B. Duke, Phys. Rev. **152**, 683 (1966); R. A. Morrow and K. R. Brownstein, Phys. Rev. B **30**, 678 (1984); H. C. Liu, Superlattices Microstruct. **3**, 413 (1987).
[22]I. V. Kukushkin *et al.*, Phys. Rev. B **40**, 4179 (1989).
[23]That is, M. Braun and U. Rössler, J. Phys. C **18**, 3365 (1985).
[24]For a review on the polaron see, e.g., J. T. Devreese and F. M. Devreese, in *Physics of the Two-Dimensional Electron Gas,* edited by J. T. Devreese and F. M. Peeters, NATO Advanced Study Institutes, Ser. B, Vol. 157 (Plenum, New York, 1987) p. 131.
[25]S. Das Sarma and B. Mason, Phys. Rev. B **31**, 5536 (1985).